Solid Earth Discuss., 6, 2885–2913, 2014
www.solid-earth-discuss.net/6/2885/2014/
doi:10.5194/sed-6-2885-2014

Solid Earth
Discussions
Open Access

Fault evolution in the Potiguar rift termination, Equatorial margin of Brazil

D. L. de Castro and F. H. R. Bezerra

Departamento de Geologia, Programa de Pós-Graduação em Geodinâmica e Geofísica, Universidade Federal do Rio Grande do Norte, Campus Universitário S/N, 59078-970 Natal, Brazil

Received: 10 September 2014 – Accepted: 19 September 2014 – Published: 2 October 2014

Correspondence to: D. L. de Castro (daavid@geologia.ufrn.br)

Published by Copernicus Publications on behalf of the European Geosciences Union.

Abstract

The transform shearing between South American and African plates in the Cretaceous generated a series of sedimentary basins on both plate margins. In this study, we use gravity, aeromagnetic, and resistivity surveys to identify fault architecture and to analyse the evolution of the eastern Equatorial margin of Brazil. Our study area is the southern onshore termination of the Potiguar rift, which is an aborted NE-trending rift arm developed during the breakup of Pangea. The Potiguar rift is a Neocomian structure located in the intersection of the Equatorial and western South Atlantic and is composed of a series of NE-trending horsts and grabens. This study reveals new grabens in the Potiguar rift and indicates that stretching in the southern rift termination created a WNW-trending, 10 km wide and ~ 40 km long right-lateral strike-slip fault zone. This zone encompasses at least eight depocenters, which are bounded by a left-stepping, en-echelon system of NW- to EW-striking normal faults. These depocenters form grabens up to 1200 m deep with a rhomb-shaped geometry, which are filled with rift sedimentary units and capped by post-rift sedimentary sequences. The evolution of the rift termination is consistent with the right-lateral shearing of the Equatorial margin in the Cretaceous and occurs not only at the rift termination, but also as isolated structures away from the main rift.

1 Introduction

The Brazilian Equatorial and West Africa margins represent a unique case of a transform plate boundary developed during the breakup of Pangea in the Cretaceous, where onshore and offshore basins were formed (Matos, 2000). As a result, a series of en echelon basins formed in the Brazilian Equatorial margin. In this context, the Neocomian Potiguar Basin, which lies at the intersection of the Eastern and Equatorial Atlantic margins of Brazil, is a key point for both piercing points (De Castro et al., 2012) and continental breakup evolution (Ponte et al., 1977; Matos, 2000).

However, despite the general knowledge of the transform margin evolution, and the Potiguar Basin in particular, several scientific gaps remain, which have important implications for the predrift misfit of the plates (Conceição et al., 1988; Unternehr et al., 1988; De Castro et al., 2012). First, some basin, such as the Potiguar Basin, has been described as failed arm of a triple junction that formed during the breakup of South America and Africa. However, they do not present plume generated magmatism (Matos, 2000). Second, most of the Precambrian fabric is NE-oriented at the margin (e.g., De Castro et al., 2012, 2014), but the Equatorial margin trends mainly EW. Third, several rifts exhibit fault systems that are not explained by an orthogonal stretching perpendicular to the rift trend (Bonini et al., 1997).

We focus on recently published regional magnetic and gravity maps of the Potiguar Basin (De Castro et al., 2012), which show areas at the SW rift boundary, whose geophysical signatures suggest the presence of unidentified buried grabens. The geophysical and geological knowledge of this rift internal geometry and boundaries were established by Bertani et al. (1990), Matos (1992) and Borges (1993), and few changes have been added to the rift architecture proposed more than 20 years ago.

Here, within the general problem of transform margins, we examine how faults evolve at rift terminations and if their geometry is inherited from basement fabric. We used a multidisciplinary geophysical survey, which included acquisition, processing and inversion of magnetic, gravity and geoelectrical data. In the present study, we investigated the architecture of these structures observed in the study by De Castro et al. (2012) at the southern onshore termination of Potiguar rift (Figs. 1 and 2). This work may provide new insights that can contribute to a better understanding of the process of continental rifts and transform margin evolution. The present study also incorporates new areas into the Potiguar rift zone.

2 Tectonic setting

The extensional deformation during the breakup of South America–Africa jumped from the eastern margin to the northwest, forming several NE-trending intracratonic basins in the Equatorial margin (Matos, 1992, 2000). The onset of this rifting in the Equatorial Atlantic occurred at ∼ 140 Ma in the Neocomian. This rifting was characterized by at the early stage of half-grabens limited by NE-trending lystric faults, which reactivated the NE-trending Precambrian fabric (Matos, 1992; Souto Filho et al., 2000). A series of NW-trending depocenters were also formed in the Equatorial margin during this period (Matos, 2000). Two dominant directions of stretching occurred: NW–SE and EW (Matos, 1992). Rifting was aborted in the early to the late Barremian, which is coeval with the oldest sediments if the African margin at the Benue basin (Matos, 1992; Nóbrega et al., 2005). After that period, the Equatorial and Southern Atlantic oceans united in the late Albian (Koutsoukos, 1992) and a subsequent thermal subsidence occurred, allowing the deposition of a transitional unit that was capped by siliciclastic and carbonate post-rift sedimentary units (Bertani et al., 1990).

The Potiguar rift, the focus of the present study, is a known structure. The onshore Potiguar rift comprises an area ∼ 150 km long and ∼ 50 km wide, with an internal geometry of asymmetric half-grabens, which are bounded by NE-trending normal faults and NW-trending transfer faults. The former reactivated, whereas the latter cut across Precambrian shear zones. The Potiguar rift is limited in the east by the Carnaubais fault, in the west by the Areia Branca hinge zone, and in the south by the Apodi fault. The main axis of the onshore Potiguar rift is NE–SW (Fig. 2) (Bertani et al., 1990). The NE–SW-oriented flat to lystric normal faults control the rift internal geometry, whereas NW–SE trending faults acted as accommodation zones and transfer faults in response to the extensional deformation (Matos, 1992).

The main depocenters reach maximum depths of 6000 m, and their basin infill was deposited in a typical continental environment (Araripe and Feijó, 1994). However, a few grabens occur away from the main depocenters. The best examples are the

Jacaúna and Messejana grabens at the western part of the Potiguar Basin (Fig. 2). They are transtensional structures bounded by E–W-trending transfer faults and NW-trending normal faults (Matos, 1992).

The rift sequence of Neocomian age is covered by a transitional Aptian marine unit, and later by the Aptian–Campanian fluvial and marine transgressive sequence, followed by the regional progradation of Paleogene clastic and carbonate deposits. These lithotypes are partially overburden by both Potiguar drift sequences and recent sedimentary cover. An angular unconformity separates the syn-rift units from the post-rift units (Souto Filho et al., 2000; Pessoa Neto et al., 2007). The siliciclastic (lower) and carbonate (upper) sequences overlap the rift zone, represented here by the Apodi and Algodões grabens (Fig. 3).

Faulting also deformed the post-rift units from the late Cretaceous to the Quaternary (Bezerra and Vita-Finzi, 2000; Kirkpatrick et al., 2013). These faults either reactivate the Precambrian shear zones and rift faults as well as cut across pre-existing structures (Bezerra et al., 2011).

3 Geophysical dataset

3.1 Magnetics

The aeromagnetic survey in the Potiguar Basin Project was flown between 1986 and 1987 by the Brazilian Petroleum Company (Petrobras) at nominal flight height of 500 m along N20° W-oriented lines spaced 2.0 km apart (MME/CPRM, 1995). We leveled and interpolated the aeromagnetic data into a 500 m grid, using the bi-directional method for the purposes of digital analysis. We further applied filtering and source detection techniques to the magnetic data such as regional-residual separation, reduction to magnetic pole, 3-D analytic signal, and 3-D Euler Deconvolution.

In addition, we carried out a magnetic ground survey along two profiles (Fig. 3) to obtain an enhanced magnetic response of the buried structures. We measured 593 sta-

tions, spaced each 40 m, using an ENVI PRO MAG (proton precession) magnetometer in the base stations and a rover G-858 (cesium vapor) magnetometer.

The reduced-to-pole residual magnetic map is marked by a rugged relief, with positive and negative anomalies of short to medium wavelengths and amplitudes that reach values of between −125 and 215 nT (Fig. 4a). The dominant magnetic trends are NE–SW-oriented, but show inflections to E–W in the W and central parts of the study area, revealing the NE–SW and E–W directions of the crystalline basement fabric. The magnetic lineaments cut across the Precambrian fabric (metamorphic foliations and shear zones) (Fig. 5). Inside the rift structures (BI, AP and AL in Fig. 4a), the magnetic surface is smooth and the anomalies are almost negative, denoting the low magnetic content of the Cretaceous sedimentary infill. A slight NW–SE oriented lineament coincides with the Apodi fault.

Figure 4b exhibits the magnetic lineaments extracted from the phase of the 3-D analytical signal and the solutions of magnetic sources location and depth analysis using the 3-D Euler Deconvolution method (Reid et al., 1990). The optimal parameters to apply the Euler Deconvolution for the study area were structural index of zero to calculate solutions for source body with contact geometry, search window size of 5.0 km and maximum tolerance of 15 % for depth uncertainty of the calculated solution. The NE–SW main magnetic trend is followed by the Euler solutions, whose sources are concentrated in depths lower than 1.5 km (Fig. 4b). It is worth mentioning that only few solutions are coincident with the rift faults. It suggests that the lateral contacts between basin structures and the basement units provide incipient contrasts of the magnetic susceptibility.

3.2 Gravity

This study integrated 1743 gravity data points (Fig. 3), which included 234 new gravity stations and 1509 data points provided by the Brazilian Petroleum Agency (ANP). This data set was interpolated with a grid cell size of 500 m using minimum curvature technique (Briggs, 1974). Afterwards, we removed the regional component from the gravity

field by applying a Gaussian regional/residual filter with a 0.8 cycles m^{-1} standard deviation. Figure 4c exhibits the resulting residual gravity map, where the NW–SE trending strips of negative anomalies mark a series of grabens. The most northwesterly gravity minimum, here named Bica graben (BI in Fig. 4), represents an extension of the Apodi graben (AP in Fig. 4). Alternatively, less dense, intrabasement gravity source could be the causative bodies for this anomaly. However, the gravity response of the Apodi graben, with NW–SE elongated minima surrounded by positive anomalies, is accurately reproduced in the Bica region. It is unlikely that basement units generated such anomaly, especially inserted in a structural framework with a main NE–SW direction (Fig. 4b). Furthermore, magnetic and geoelectrical data also corroborate the presence of a thickened basin infill in this area, since the magnetic anomalies and Euler solutions show no intrabasement source and the geoelectrical sections indicate a deeper contact between the less resistive sedimentary sequence and more resistive crystalline basement (see Sect. 3.3 below).

In the SE portion of the study area, the Algodões graben comprises two gravity minima, separated by a slight positive anomaly (AL in Fig. 4c). The 20 km long gravity low is oriented to NW–SE direction parallel to the main trend of the Bica and Apodi grabens. The gravity anomalies suggest that the eastern segment of the rift is extended southeastwards in comparison with the limits drawn by Borges (1993) based on reflection seismic lines. Others short wavelength gravity minima occur in the NW and NE parts of the study area (Fig. 4c). Nevertheless, the presence of a graben is not expected in those cases. Lack of an appropriate stations coverage in those areas, different gravity trends and partially outcropped granitic and supracrustal units lead us to such an interpretation.

Figure 4d exhibits the gravity lineaments extracted from the residual anomaly map and the solutions of gravity source detection using the 3-D Euler Deconvolution method. The Euler Deconvolution parameters applied to gravity data are the same applied to the magnetic data. Differently from the magnetic case, the gravity lineaments preferentially trend to the NW–SE direction, following the main rift faults. In turn, the

Euler solutions reveal narrow (less than 1500 m depth) gravity sources oriented in the NW–SE direction in the rift zone (shaded area in Fig. 4d). The faulted borders of the grabens are delimited by the Euler solutions. On the other hand, Euler solutions are oriented to N–S and E–W in the SW and northern parts of the study area, respectively. Some of these solutions are related to the intrabasement gravity sources and structures, but most of them are biased by the scarce and irregular distribution of gravity stations, concentrated along roads (Fig. 3).

3.3 Geoelectrical sounding

Seventeen geoelectrical surveys were carried out along two profiles crossing the rift structures (P01 and P02 in Figs. 3 and 4). The vertical electrical soundings (VES) were measured to define different geoelectrical layers and the internal geometry of the grabens. The soundings were spaced 2.0 to 3.0 km and all measurements were taken using Schlumberger electrode array with current electrode half spacing (AB/2) ranging between 1.5 and 1200 m. The resistivity equipment comprises a DC-DC converter 12/1000, with maximum power of 500 W, and a digital potential receiving unit, which were able to provide the apparent resistivity with high accuracy.

We constructed two geoelectrical pseudo-sections using the resistivity measurements and the half spacing between the current electrodes (Fig. 6). The study indicates four geoelectrical units in both sections. The deepest unit represents the crystalline basement with a resistivity up to 50 Ω m Directly overlying the bedrock occurs a low resistive layer (< 35 Ω m), which is interpreted as the siliciclastic rift unit (Pendência Formation). In Profile P01, the lateral increase of resistivity between VES 8 and 9 indicates the faulted border of the Bica graben and, consequently, the SE limit of this geoelectrical layer (Fig. 6a). The geoelectrical layers show a generalized increase in resistivity from this area as far as the SE end of Profile 01 and in all Profile 02. This pattern could be explained as a decrease in the moisture content caused by the presence of a low permeable carbonate layer on the top of the sedimentary infill. Along

Profile 02, the rift sequence reaches its highest thickness in the Algodões depocenter between VES 13 and 16 (Fig. 6b).

The intermediary geoelectrical layer is characterized by very low resistivities (< 18 Ω m), where the siliciclastic unit of the post-rift sequence outcrops (Figs. 3 and 6). In the SE part of Profile 01 (VES 8 to 11), the layer resistivity reaches 55 Ω m, where it is overlapped by a more resistive layer (> 140 Ω m), the carbonate unit. Its thickness varies slightly along Profile 01, whereas this layer is thicker over the main depocenter in Profile 02 (Fig. 6), suggesting local reactivation of rifting faults during carbonate deposition in the post-rift phase. The uppermost carbonate unit also exhibits a thickening in the Algodões rift zone along Profile 02.

4 Gravity-geoelectric joint inversion

We applied an algorithm developed by Santos et al. (2006) in two transects, crossing the Bica (P01) and Algodões (P02) grabens (Figs. 3 and 4) to identify the resistivity interfaces and subsurface electrical resistivity distribution within the rifting areas. This algorithm is based on simulated annealing technique to jointly invert gravity and resistivity (vertical electrical soundings – VES) data for mapping the internal architecture of the basin and its layered infill. Using seismic and well log data to constrain this joint-inversion procedure, De Castro et al. (2011) obtained good results for the rift internal architecture applying the Santos algorithm in a regional transect across the Potiguar Basin.

Gravity lows suggest asymmetric semi-grabens with depocenters located between 10 and 20 km and 2.5 and 10 km in the P01 and P02, respectively (Fig. 7a and d). The footwalls are represented by magnetic maxima and the depocenters by negative magnetic anomalies (Fig. 7b and e). We also calculated a 2-D Euler deconvolution along the profiles (Fig. 7c and f) to guide the gravity-geoelectrical joint inversion, providing the expected rift geometries and locations of intrabasement heterogeneities. The structural indexes of 0.5 to gravity and 2.0 to magnetic data are the best ones to describe the

expected behavior of the faulted borders of the grabens in depth. The structural index of 0.5 applied to magnetic data is more suitable to indicate basement heterogeneities.

In Transect P01, the alignment pattern of gravity Euler solutions marks the both NW and SE edges of the Bica graben (crosses in Fig. 7c). This set of gravity Euler solutions suggests an asymmetric semi-graben in agreement with the geoelectrical section (Fig. 6). Unlike, clouds of magnetic Euler solutions indicate shallow causative sources within the basin (circles in Fig. 7c), albeit few solutions are coincident with gravity Euler solutions at the SE limit of the graben. A similar result was obtained in the Algodões graben (Profile P02 in Fig. 7). However, the gravity Euler solutions are flatter than expected for the fault that limits the NW rift edge, which suggest that the border faults of the rift exhibits a low dip angle. Additionally, magnetic Euler solutions mark intrabasement sources at the graben shoulders (red circles in Fig. 7f).

In order to apply the joint inversion, we adopted a four-layer model for Transect P01, representing the basement, rift and post-rift units, and a thin soil layer. In Profile P02, the uppermost post-rift sequence could be divided into two layers, since the siliciclastic and carbonate units are well defined along all VES (Fig. 6b). Each layer was discretized in 31 (Profile 01) or 17 (Profile 02) cells with widths of 1.0 km. At both ends of the profile, the cells are extended 10 km to avoid edge effects in the calculated gravity anomalies. The density values of the layers were, from base to top: 2.75 g cm^{-3} for the bedrock (basement), 2.50 g cm^{-3} (rift sequence), 2.30 g cm^{-3} (siliciclastic unit), 2.45 g cm^{-3} (carbonate unit), and 2.00 g cm^{-3} (superficial dry soil). In Profile 01, a density of 2.35 g cm^{-3} was assumed for the post-rift unit, encompassing the siliciclastic and carbonate units. We performed 25 density measurements on selected samples that represented sedimentary and basement rocks. Densities obtained by De Castro (2011) in the well logs located at the eastern border of the Potiguar rift were also considered in the models. The density measurements increase with depth and may represent sediment compaction.

Initially, a 1-D inversion method was applied in each VES to obtain estimates of the resistivity of the 2-D model layers, as well to establish search limits of resistivity and

depth for each model cell. Estimates of the resistivity and thickness values were calculated from the original data by using the IPI2Win software developed by Bobachev (2003). The inversion process uses a variant of the Newton algorithm of the least number of layers or the regularized fitting minimizing algorithm using Tikhonov's approach to solve incorrect problems. Iterations using this code were carried out automatically and interactively (semi-automated) until the calculated model satisfied a minimum difference between measured and calculated data.

Figures 8 and 9 present the internal geometry and density-resistivity distribution of the final models obtained by the joint inversion for each profile. In general, both gravity and geoelectric data have good degrees of fit in comparison with the calculated gravity anomaly and DC curves, respectively. The grabens identified in the geoelectrical sections (Fig. 6) and by gravity Euler solutions (Fig. 7) were reconstituted by gravity-geoelectric modelling. In Profile P01, the SE border of the Bica half-graben, revealed by the calculated model, is controlled by a normal fault with 40° dip and vertical offset of almost 1200 m (Fig. 8). A basement high bounds the 8 km wide main depocenter to the NW. Outside the rift, the basin infill sharply decreases to less than 200 m thick. The post-rift unit exhibits a slight thickening northwestward (Ca/Si in Fig. 8). Likewise, the Algodões graben shows asymmetric half-graben geometry, reaching a maximum depth of 1150 m (Fig. 9). However, the post-rift siliciclastic unit is thickened on the central portion of the rift (Si in Fig. 9), unlike the flattened post-rift deposition in the Bica graben, which suggest a tectonic reactivation in the Algodões graben during the deposition of the post-rift unit.

5 3-D gravity modelling

The study employed a 3-D model of the gravity anomaly that used the approach proposed by De Castro et al. (2007). The algorithm simulates gravity anomalies of vertical rectangular prisms in the observed field using a quadratic function to account the increase in density with depth within the basin (Rao and Babu, 1991). The new approach

used here takes into account the possibility that basement rocks that underlie sedimentary basins have variable density. This approach separates basin and basement gravity during the modeling process, which provides the shape of the low-density basin, without the gravity effects of the heterogeneous basement (Jachens and Moring, 1990; Blakely, 1996).

The calculated thickness of basin-filling deposits depends on the density-depth function used in the modelling (Blakely et al., 1999). In the study area, the coefficients of the density function within the basin were fitted by the least-square method, which were extracted from the joint-inverted final density models. Nevertheless, the linear coefficient of the quadratic function represents the density contrast in surface and guides the modeling process. The chosen superficial contrast was $-0.27\,\mathrm{g\,cm^{-3}}$, which provides good agreement with joint-inverted models (Figs. 8 to 10 and Table 1). However, the calculated depths of this 3-D model do not match with the basin infill thickness at exploratory wells in the Apodi graben (location in Figs. 3, 4, and 10). Using a lower density contrast ($-0.20\,\mathrm{g\,cm^{-3}}$) the resulting gravity model provided depths for the basement top that is consistent with depth found in the exploratory Well 3 (Table 1). The high misfit for Well 1 points that the density contrast increases westward to the Apodi graben boundary, getting closer to the density dataset for the Bica graben. In summary, gravity modelling reveals that the densities are higher where the basin infill is thicker, probably due to more intense sediment compaction in these areas. Since the major interest of this research is focused on the Bica and Algodões grabens, Fig. 10 shows the 3-D gravity model obtained using the density contrast of $-0.27\,\mathrm{g\,cm^{-3}}$, which was more consistent with the results of the joint inversion. Assuming a basement density of $2.75\,\mathrm{g\,cm^{-3}}$, the modelling yielded average densities of these sedimentary units of about $2.48\,\mathrm{g\,cm^{-3}}$.

6 Architecture and kinematics of the Potiguar rift termination

The present study indicates that the southern termination of the main rift is more complex than the previous investigations have indicated. The analysis of the magnetic lin-

eaments and the basement foliation and shear zones indicate that the basement fabric did not exert control in fault geometry at the rift termination, as already observed in the NE-trending lystric faults by De Castro et al. (2012) along the main rift. The new rift termination is characterized by a WNW-trending, 10 km wide and ∼ 40 km long fault zone. Inside this fault zone, stretching created a series of NW–SE-trending left-stepping en echelon depocenters. Based on gravity maps, we interpreted the depocenters to exhibit an en echelon geometry and fault segments 35 km long.

The depocenters form two main grabens, the Algodões and the Bica grabens. The former was described by Matos (1992), whereas the latter is a new structure presented for the first time in the present study. Both grabens are separated from the main rift by horsts and their main axes are at high angle to the NE-trending Potiguar rift. Both grabens are composed of a syn-rift and post-rift sedimentary units. The syn-rift units are bounded by rift faults, whereas the post-rift units cap the whole basin. In addition, both grabens do not exhibit present-day topographic expression and most of the faults that cut across the rift units die out in the post-rift layers.

The 3-D gravity model reveals a NW trending rift geometry for the Bica graben (BI in Fig. 10), beyond the previous mapped limits of the Potiguar rift. This graben is ∼ 30 km long and ∼ 15 km wide, and is limited by segmented NW-trending oblique-slip faults. NS-oriented, en echelon faults split the graben into four depocenters, whose greatest thickness reaches 1130 m. One of these rift borders is the Apodi fault (2 in Fig. 2), previously described in the study of Bertani et al. (1990) as a normal fault. The Mulungu fault was also identified by Bertani et al. (1990) and Matos (1992) (1 in Fig. 2). This rift geometry is roughly similar to the internal architecture of the Apodi graben (AP in Fig. 10). The Algodões graben comprises an E–W trending structure 25 km long and 8 km wide, which bends to NW–SE direction in its eastern part (AL in Fig. 10). As in others grabens, the Apodi fault system also exerts structural control on the northern rift border. Furthermore, an incipient basement high separates the Algodões graben into two depocenters. The occurrence of this structure is well recorded in the magnetic, gravity and geoelectrical data (Figs. 4 and 6). The local basin infill is 1050 m deep.

The deformation was partitioned between the WNW-striking rift strike-slip faults and the internal N–NW-striking, en echelon normal faults. The lack of surface expression of the faults in the study area indicates that they were mainly active during rifting. The study also indicates that the WNW-trending faults that border the Bica and Algodões grabens and their relationship with the NS-trending faults are consistent with an oblique-slip dextral component of displacement of the former. The NS-trending en echelon faults occur in both grabens and are consistent with this oblique-slip dextral component movement of the WNW-striking faults. The maximum vertical throws of the NW-trending border faults are ∼ 1100 m and they decrease eastward in the Algodões graben and westward in the Bica graben (Fig. 10). Both fault sets indicate that the structures were formed by transtensional shearing.

7 Discussion

The reactivation of the Precambrian fabric originated the main NE-trending rift fault (De Castro et al., 2012). In this context, the pre-existing fabric in the upper lithosphere exerts the main control of fault reactivation during continental rifting (De Castro et al., 2012). However, this study indicates that the southern rift termination cut across the existing Precambrian fabric. The en echelon depocenters in the southern rift termination are consistent with the syn-transtentional phase of the Equatorial margin (Matos, 2000), which also cut across the pre-existing basement fabric along the margin.

The Potiguar rift experienced two phases of extension: the first was a NW-trending extension in the Neocomian and the second was an E–W-trending rift extension in the Barremian (Matos, 1992). The stretching observed at the Potiguar rift in the present study is consistent with this second phase of rift extension, which suggests that this rift termination developed after the main rift trend was aborted (Matos, 1992). This rift termination also coincides with the development of the Jacaúna and Messejana grabens (Fig. 2), which were formed by EW-trending extension (Matos, 1992), and with the onset of rifting in the Equatorial margin (Matos, 2000).

Crustal extension in the first rift phase was distributed across the NE-trending rift faults of the Potiguar rift. During the evolution of the Potiguar rift termination, fault movement was partitioned between the master faults and the internal graben faults. This pattern of rift termination is different from the one observed at the other small basins to the south of the Potiguar rift, where the rift border and intra-rift faults are roughly orthogonal to the rift stretching (De Castro et al., 2007, 2008).

The dextral shear of the border faults of the small grabens adjacent and to the west of the Potiguar main rift roughly coincides with the major transform movement of Africa and South America along the Equatorial margin. The transtension of the Equatorial margin is consistent with the NW-trending depocenters and right-lateral shear of the southern termination of the Potiguar rift.

8 Conclusions

Previous studies indicate that the Potiguar rift lies in the intersection of the Equatorial margin and the eastern margin of South America and is overburden by the post-rift sedimentary units. It encompasses a series of NE-trending horsts and grabens. This study extends the investigation of previous works by focusing on the fault evolution at the rift termination using gravity, magnetic, and resistivity data. This study indicates that stretching of the southern end of the Potiguar rift was accommodated by both a ∼ 40 km long strike-slip and a system of minor left-stepping en echelon normal faults. We documented two small rhomb-shaped grabens at the rift termination. They are NW-trending full-grabens developed during oblique rifting. The grabens were developed along NW-trending oblique-slip faults. Depocenters in the grabens were split by en echelon NS-trending normal faults. Faults of these grabens die out in the post-rift sedimentary units. The rifting coincided with the development of the Equatorial margin, which was subjected to right-lateral transform movement during this period.

Acknowledgements. This study was suported by the Brazilian Research Council (CNPq) – Project N. 470891/2010-6. The authors thank the Brazilian Geological Survey (CPRM) for supplying airborne magnetic data and CNPq for their PQ grants.

References

Angelim, L. A. A., Medeiros, V. C., and Nesi, J. R.: Programa Geologia do Brasil – PG B. Projeto Mapa Geológico e de Recursos Minerais do Estado do Rio Grande do Norte. Mapa Geológico do Estado do Rio Grande do Norte. Escala 1 : 500 000, Recife: CPRM/FAPERN, 2006.

Araripe, P. T. and Feijó, F. J.: Bacia Potiguar, Boletim de Geociências da Petrobras, 8, 127–141, 1994.

Bertani, R. T., Costa, I. G., and Matos, R. M. D.: Evolução tectono-sedimentar, estiloestrutural e habitat do petróleo na Bacia Potiguar, in: Origem e evolução de Bacias Sedimentares, edited by: Gabaglia, G. P. R. and Milani, E. J., Petrobras, Rio de Janeiro, 291–310, 1990.

Bezerra, F. H. R. and Vita-Finzi, C.: How active is a passive margin? Paleoseismicity in northeastern Brazil, Geology, 28, 591–594, 2000.

Bezerra, F. H. R., Do Nascimento, A. F., Ferreira, J. M., Nogueira, F. C. C., Fuck, R. A., Brito Neves, B. B., and Sousa, M. O. L.: Review of active faults in the Borborema Province, Intraplate South America Integration of seismological and paleoseismological data, Tectonophysics, 510, 269–290, 2011.

Blakely, R. J.: Potential Theory in Gravity and Magnetic Applications, 2nd edn., Cambridge University Press, London, 441 pp., 1996.

Blakely, R. J., Jachens, R. C., Calzia, J. P., and Langenheim, V. E.: Cenozoic basins of the Death Valley extended terrane as reflected in regional-scale gravity anomalies, Geological Society of America Special Paper, 333, 16, 1999.

Bobachev, A.: IPI2Win-1D automatic and manual interpretation software for VES data, available at: geophys.geol.msu.ru/ipi2win.htm, 2003.

Bonini, M., Souriot, T., Boccaletti, M., and Brun, J. P.: Successive orthogonal and oblique extension episodes in a rift zone: laboratory experiments with application to the Ethiopian Rift, Tectonics, 16, 347–362, 1997.

Borges, W. R. E.: Caracterização Estrutural daPorção SW do Rifte Potiguar, M.S. thesis, Universidade Federal de Ouro Preto, Ouro Preto, Brazil, 146 pp., 1993.
Briggs, I. C.: Machine contouring using minimum curvature, Geophysics, 39, 39–48, 1974.
Conceição, J. C. J., Zalán, P. V., and Wolff, S.: Mecanismo, Evolução e Cronologia do Rift Sul-Atlântico, Boletim de Geociências da PETROBRAS, 2, 255–265, 1988.
De Castro, D. L.: Gravity and magnetic joint modeling of the Potiguar rift basin (NE Brazil): basement control during Neocomian extension and deformation, J. S. Am. Earth Sci., 31, 186–198, 2011.
De Castro, D. L., Bezerra, F. H. R., and Castelo Branco, R. M. G.: Geophysical evidence of crustal-heterogeneity control of fault growth in the Neocomian Iguatu basin, NE Brazil, J. S. Am. Earth Sci., 26, 271–285, 2008.
De Castro, D. L., Oliveira, D. C., and Castelo Branco, R. M. G.: On the Tectonics of the Neocomian Rio do Peixe rift basin, NE Brazil: lessons from gravity, magnetics and radiometric data, J. S. Am. Earth Sci., 24, 186–202, 2007.
De Castro, D. L., Pedrosa, N. C., and Santos, F. A. M.: Gravity-geoelectric joint inversion over the Potiguar rift basin, NE Brazil, J. Appl. Geophys., 75, 431–443, 2011.
De Castro, D. L., Bezerra, F. H. R., Sousa, M. O. L., and Fuck, R. A.: Influence of Neoproterozoic tectonic fabric on the origin of the Potiguar Basin, northeastern Brazil and its links with West Africa based on gravity and magnetic data, J. Geodyn., 54, 29–42, 2012.
De Castro, D. L., Fuck, R. A., Phillips, J. D., Vidotti, R. M., Bezerra, F. H. R., and Dantas, E. L.: Crustal structure beneath the Paleozoic Parnaíba Basin revealed by airborne gravity and magnetic data, Brazil, Tectonophysics, 614, 128–145, 2014.
Jachens, R. C. and Moring, B. C.: Maps of thickness of Cenozoic deposits and the isostatic residual gravity over basement for Nevada, US Geological Survey Open-File Report 90–404, scale 1 : 1 000 000, 1990.
Kirkpatrick, J. D., Bezerra, F. H. R., Shipton, Z. K., Do Nascimento, A. F., Pytharouli, S. I., Lunn, R. J., and Soden, A. M.: Scale-dependent influence of pre-existing basement shear zones on rift faulting: a case study from NE Brazil, J. Geol. Soc. London, 170, 237–247, 2013.
Koutsoukos, E. A. M.: Late Aptian to Maastrichtian foraminiferal biogeography and palaeoceanography of the Sergipe basin, Brazil, Palaeogeogr. Palaeocl., 92, 295–324, 1992.
Matos, R. M. D.: The northeast Brazilian rift system, Tectonics, 11, 766–791, 1992.

Matos, R. M. D.: Tectonic evolution of the equatorial South Atlantic, Geophysical Monography AGU, 115, 331–354, 2000.
MME/CPRM: Catálogo General de Produtos e Serviços, Geologia, Levantamentos Aerogeofísicos – Database AERO, Rio de Janeiro, 359 pp., 1995.
Moulin, M., Aslanian, D., and Unternehr, P.: A new starting point for the South and Equatorial Atlantic Ocean, Earth-Sci. Rev., 98, 1–37, 2010.
Nóbrega, M. A., Sa, J. M., Bezerra, F. H. R., Hadler Neto, J. C., Iunes, P. J., Oliveira, S. G., Saenz, C. A. T., and Lima Filho, F. P.: The use of apatite fission track thermochronology to constrain fault movements and sedimentary basin evolution in northeastern Brazil, Radiat. Meas., 39, 627–633, 2005.
Pessoa Neto, O. C., Soares, U. M., Silva, J. G. F., Roesner, E. H., Florência, C. P., and Souza, C. A. V.: Bacia Potiguar, Boletim de Geociências da Petrobras, 15, 357–369, 2007.
Ponte, F. C., Fonseca, J. R., and Morales, R. E.: Petroleum geology of the eastern Brazilian Continental Margin, AAPG Bull., 61, 1470–1482, 1977.
Rao, D. B. and Babu, N. R.: A Fortran-77 computer program for three-dimensional analysis of gravity anomalies with variable density contrast, Comput. Geosci., 17, 655–667, 1991.
Reid, A. B., Allsop, J. M., Granser, H., Millet, A. J., and Somerton, I. W.: Magnetic interpretation in three dimensions using Euler deconvolution, Geophysics, 55, 80–91, 1990.
Santos, F. A. M., Sultan, S. A., Represas, P., and El Sorady, A. L.: Joint inversion of gravity and geoelectrical data for groundwater and structural investigation: application to the northwestern part of Sinai, Egypt. Geophys. J. Int., 165, 705–718, 2006.
Souto Filho, J. D., Correa, A. C. F., Santos Neto, E. V., and Trindade, L. A. F.: Alagamar-Açu petroleum system, onshore Potiguar Basin, Brazil: a numerical approach for secondary migration, in: petroleum systems of South Atlantic margins, AAPG Memoir, 73, 151–158, 2000.
Unternehr, P., Curie, D., Olivet, J. L., Goslin, J., and Beuzart, P.: South Atlantic fits and intraplate boundaries in Africa and South America, Tectonophysics, 155, 169–179, doi:10.1016/0040-1951(88)90264-8, 1988.

Table 1. Comparison between the depths to basement obtained from joint-inverted approach (A) and in exploratory wells (B) and those depths obtained by the 3-D gravity modeling using density contrast of $-0.27\,g\,cm^{-3}$ (C) and $-0.20\,g\,cm^{-3}$ (D) and the respective misfits.

Graben	Location	Depth (m)					
		A	B	C	Misfit (%)	D	Misfit (%)
Bica	Profile P01	1110	–	1130	1.8	5902	431.7
Algodões	Profile P02	1030	–	1050	1.9	5446	428.7
Apodi	Well 1	–	1898	720	62.1	4622	143.5
	Well 2	–	> 3703	709	–	4300	–
	Well 3	–	4424	881	80.1	4865	9.9

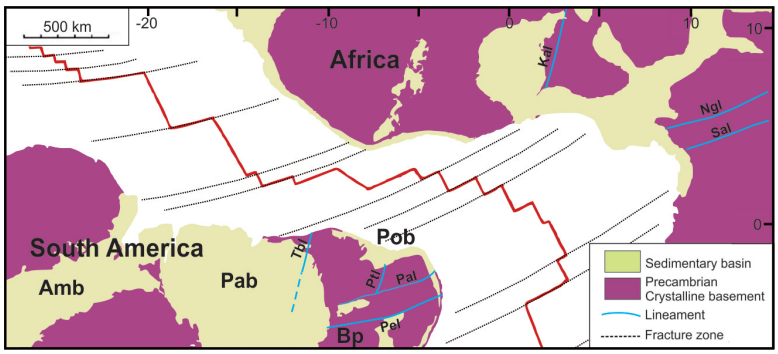

Figure 1. Schematic reconstruction of northeastern Brazil and western Africa at Cron C34 (red line) showing the main pre-drift piercing point and sedimentary basins (Amb – Amazon, Pab – Parnaíba; Pob – Potiguar) in both margins (Adapted from Moulin, 2010). Bp – Borborema Province; Precambrian lineaments: Tbl – Transbrasiliano; Ptl – Portalegre; Pal – Patos; Pel – Pernambuco; Kal – Kandi; Ngl – Ngaoundere; Sal – Sanaga.

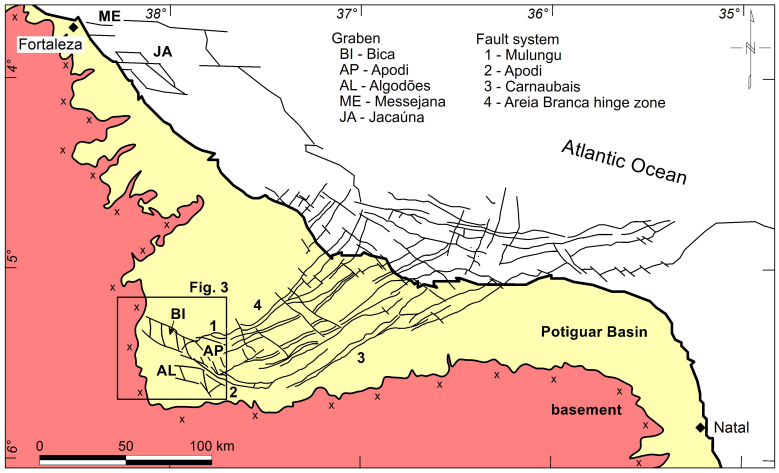

Figure 2. Simplified geologic map of the Potiguar Basin in NE Brazil (adapted from Angelim et al., 2006). The rift structures in the maps of Figs. 2 and 4 are inferred from interpretation of seismic sections and well logs, conducted by Matos (1992) and Borges (1993). The grabens located at the SW rift termination are derived from the present geophysical survey.

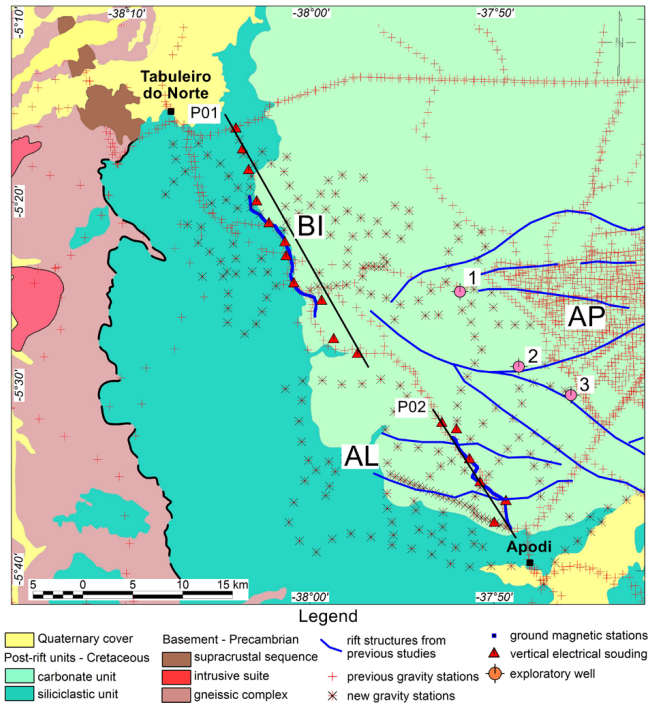

Figure 3. Geologic map of the SW border of the Potiguar Rift with the location of the geophysical datasets. (Grabens: BI – Bica, AP – Apodi and AL – Algodões; Profiles: P01 and P02; Exploratory wells: 1, 2 and 3).

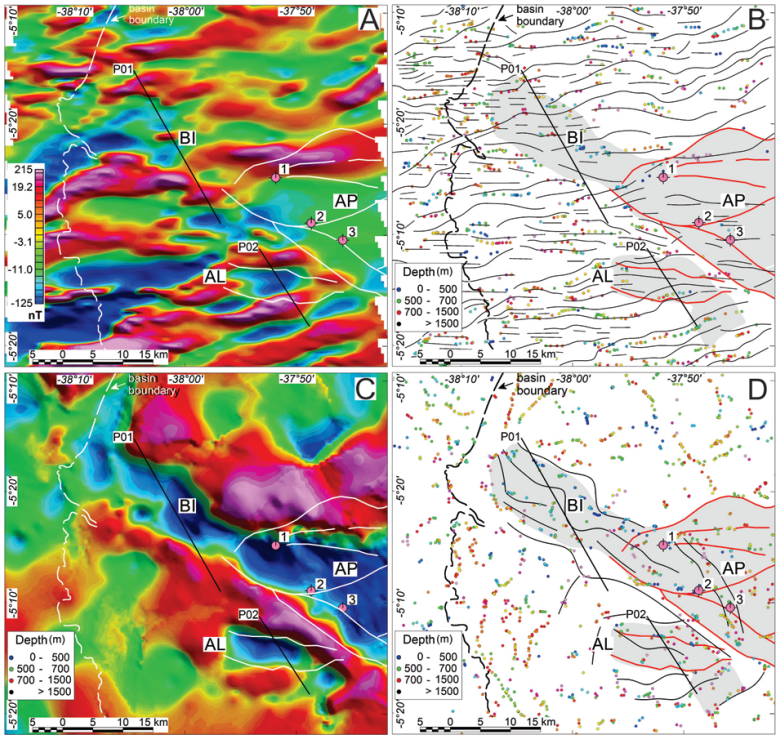

Figure 4. (A) Residual component of the magnetic field reduced to the pole and **(B)** major magnetic lineaments and Euler solutions; **(C)** Residual gravity anomaly map and **(D)** major gravity lineaments and Euler solutions. (Grabens: **(A)** – Bica, **(B)** – Apodi and **(C)** – Algodões; Profiles: P01 and P02; Exploratory wells: 1, 2 and 3). White and red traces: rift structures from previous studies.

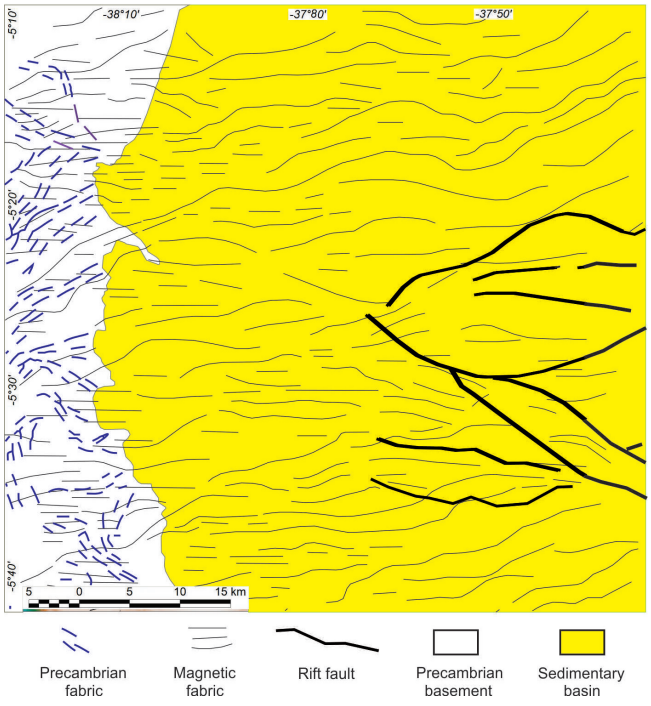

Figure 5. Comparison between Precambrian structural fabric derived from remote sensing and NE–SW to E–W trending magnetic lineaments.

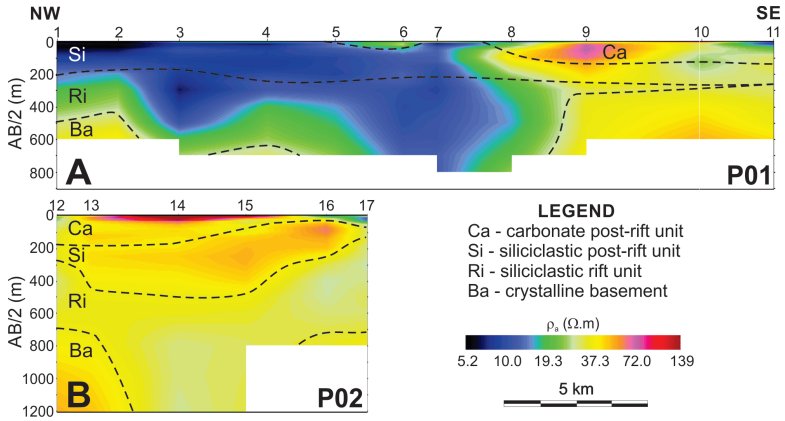

Figure 6. Interpreted apparent resistivity cross sections of profiles P01 (top) and P02 (bottom).

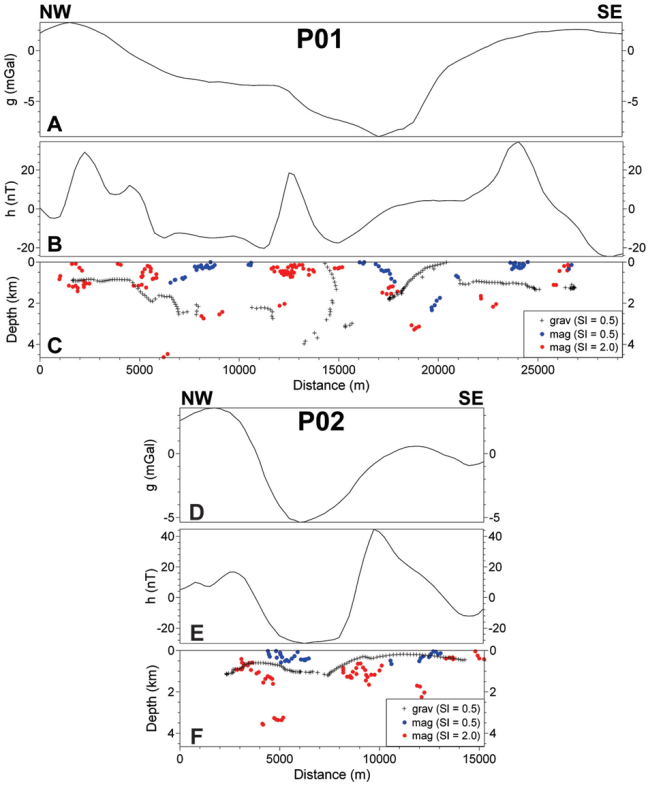

Figure 7. Gravity **(A, D)** and magnetic **(B, E)** anomalies and Euler solutions **(C, F)** of profiles P01 (top) and P02 (bottom).

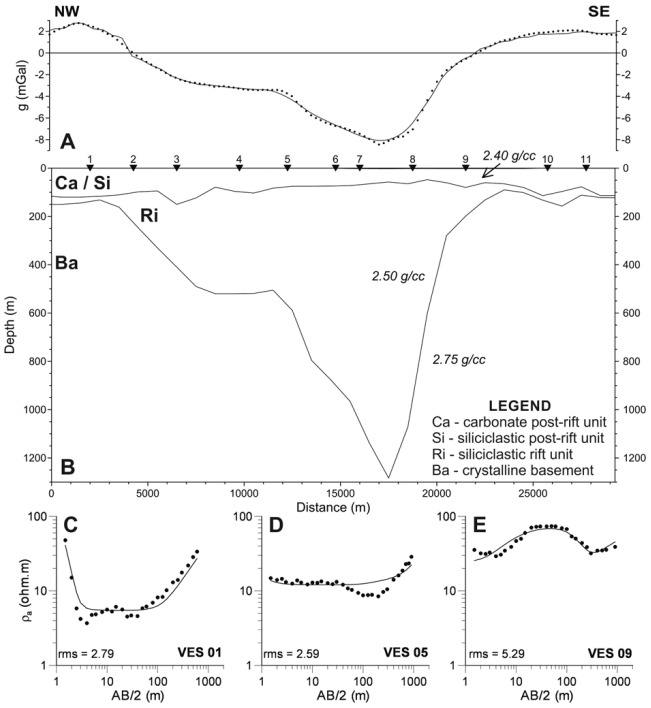

Figure 8. Observed (dots) and calculated (solid line) gravity anomaly across the Profile P01 **(A)** and the final model response obtained from joint inversion method **(B)**. Comparison of three VES data (dots) and model responses of the gravity–geoelectric joint inversion (**C** to **E**). rms: VES misfit (per cent).

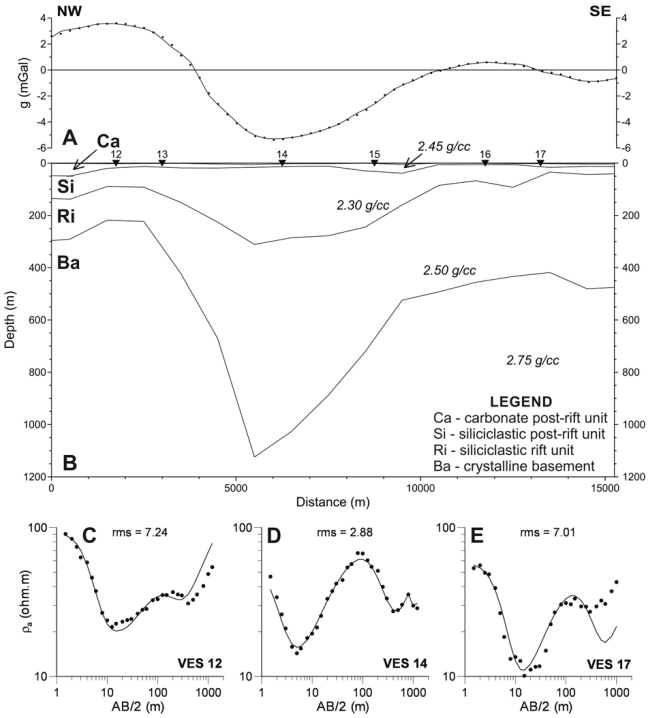

Figure 9. Observed (dots) and calculated (solid line) gravity anomaly across the Profile P02 **(A)** and the final model response obtained from joint inversion method **(B)**. Comparison of three VES data (dots) and model responses of the gravity–geoelectric joint inversion (**C** to **E**). rms: VES misfit (per cent).

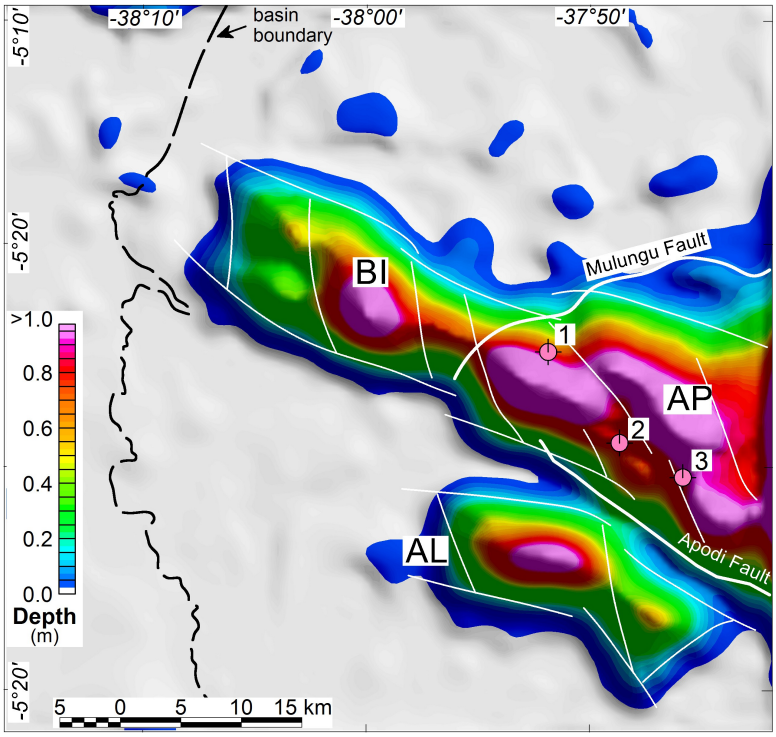

Figure 10. Basement contour map of the SW border of the Potiguar Rift derived from 3-D-gravity modeling with major fault segments (thin white traces). Thick white traces: rift structures from previous studies. Grabens: BI – Bica, AP – Apodi and AL – Algodões.